

Scaling of global properties of fluctuating and mean streamwise velocities in pipe flow: Characterization of a high Reynolds number transition region

Cite as: Phys. Fluids **33**, 065127 (2021); doi: 10.1063/5.0054769

Submitted: 21 April 2021 · Accepted: 2 June 2021 ·

Published Online: 28 June 2021



View Online



Export Citation



CrossMark

Nils T. Basse^{a)}

AFFILIATIONS

Independent Scientist, Trubadurens väg 8, 423 41 Torslanda, Sweden

^{a)} Author to whom correspondence should be addressed: nils.basse@npb.dk

ABSTRACT

We study the global, i.e., radially averaged, high Reynolds number (asymptotic) scaling of streamwise turbulence intensity squared defined as $I^2 = \overline{u^2}/U^2$, where u and U are the fluctuating and mean velocities, respectively (overbar is time averaging). The investigation is based on the mathematical abstraction that the logarithmic region in wall turbulence extends across the entire inner and outer layers. Results are matched to spatially integrated Princeton Superpipe measurements [Hultmark *et al.*, “Logarithmic scaling of turbulence in smooth- and rough-wall pipe flow,” *J. Fluid Mech.* **728**, 376–395 (2013)]. Scaling expressions are derived both for log- and power-law functions of radius. A transition to asymptotic scaling is found at a friction Reynolds number $Re_\tau \sim 11\,000$.

Published under an exclusive license by AIP Publishing. <https://doi.org/10.1063/5.0054769>

I. INTRODUCTION

We have studied the scaling of streamwise turbulence intensity (TI) with Reynolds number in Refs. 1–3 and continue our research in this paper. We define the square of the TI as $I^2 = \overline{u^2}/U^2$, where u and U are the fluctuating and mean velocities, respectively (overbar is time averaging). Physically, the square of the TI is equal to the ratio of the fluctuating and mean kinetic energy. The square of the normalized fluctuating velocity is $\overline{u^2}/U_\tau^2$, where U_τ is the friction velocity. In the literature, the square of the normalized fluctuating velocity is sometimes called the TI. The square of the normalized mean velocity is U^2/U_τ^2 .

As before, we use publicly available measurements from the Princeton Superpipe.^{4,5}

In previous work, we have studied the global, i.e., radially averaged TI and attempted to fit the measurements to equations with two parameters, either log- or power-laws. We have assumed that the same scaling expression is valid for all Reynolds numbers measured.

Now, we go one step further and assume that $\overline{u^2}/U_\tau^2$ and U^2/U_τ^2 can be expressed separately as two-parameter functions of the distance from the wall, either as log- or power-laws. This approach provides the parameters as a function of Reynolds number, thereby allowing us to answer the question whether they depend on Reynolds number or

not. The log-law is based on the description in Ref. 6, and the power-law has a functional form which is equivalent to the log-law in the sense that

$$x^{1/a} = \exp(\log(x)/a) \simeq 1 + \frac{\log(x)}{a}, \quad (1)$$

where a is a constant, x is a variable, and the approximation is valid for $\log(x)/a \ll 1$. We make the assumption that the log- and power-law hold across the entire inner and outer layers. For the log-law, this assumption is known to be unphysical outside the logarithmic region.

An important motivation for our work are the applications to computational fluid dynamics (CFD) simulations,⁷ where the TI is often used as a boundary condition. Recently, a machine learning deep neural network was applied to estimate the TI from short duration velocity signals.⁸ This approach may lead to novel information on the temporal variation of the TI scaling behavior.

The paper is organized as follows: In Sec. II, we briefly summarize the importance of the TI as a boundary condition for CFD simulations. Thereafter, we review the local logarithmic velocity scaling in Sec. III, followed by global log- and power-law scaling results in Sec. IV. We discuss our findings in Sec. V and conclude in Sec. VI.

II. TURBULENCE INTENSITY AS A CFD BOUNDARY CONDITION

A canonical example of a turbulence model where the TI is used as a boundary condition is the standard $k - \varepsilon$ model⁹ where two equations are solved, one for the turbulent kinetic energy (TKE) k and another for the rate of dissipation of the TKE, ε ,

$$k = \frac{3}{2}(U_{\text{ref}}I)^2, \tag{2}$$

$$\varepsilon = C_\mu^{3/4} \frac{k^{3/2}}{l}, \tag{3}$$

where U_{ref} is a characteristic velocity, $I^2 = \overline{u^2}/U_{\text{ref}}^2$ is the TI, C_μ is a dimensionless constant, and l is a characteristic length. We return to length scales in Sec. V C.

Thus, we see that a reliable estimate of the TI is needed to calculate the TKE.

The kinematic turbulent viscosity is assumed to be isotropic and defined as

$$\nu_t = C_\mu \frac{k^2}{\varepsilon} = C_\mu^{1/4} l \sqrt{3/2} U_{\text{ref}} I. \tag{4}$$

An expression often used for the TI is one contained in the documentation of a commercial CFD software,¹⁰

$$I = 0.16 \times Re_{D_H}^{-1/8}, \tag{5}$$

where Re_{D_H} is the Reynolds number based on the hydraulic diameter D_H . No reference is supplied, but the statement above the equation reads:

“The turbulence intensity at the core of a fully developed duct flow can be estimated from the following formula derived from an empirical correlation for pipe flows.”

Note that other commercial (and open-source) CFD codes also use Eq. (5), e.g., Ref. 11. We find that problematic since the origins of the equation are unclear and no references are provided. Our research aims to remedy the situation by modeling the TI using publicly available measurements.

III. LOCAL SCALING

We first write the log-law for the streamwise mean velocity as formulated in Ref. 6,

$$U_l^+(z) = \frac{1}{\kappa_l} \log(z^+) + A_l \tag{6}$$

$$= \frac{1}{\kappa_l} \log(z/\delta) + \frac{1}{\kappa_l} \log(Re_\tau) + A_l, \tag{7}$$

where $U_l^+ = U_l/U_\tau$, U_l is the mean velocity in the streamwise direction, $z^+ = zU_\tau/\nu$ is the normalized distance from the wall, z is the distance from the wall, ν is the kinematic viscosity, κ_l is the von Kármán constant, and A_l is a constant for a given wall roughness. Note that

$$z/\delta = \frac{z^+}{Re_\tau}, \tag{8}$$

where $Re_\tau = \delta U_\tau/\nu$ is the friction Reynolds number and δ is the boundary layer thickness (pipe radius R for pipe flow). The subscript “ l ” means that the constants are “local” fits, i.e., the range of z where

the log-law describes the measurements well (logarithmic region). Although the log-law is not valid close to the wall, we observe that $U_l^+ = 0$ if $z_l^+ = \exp(-A_l \kappa_l)$. For the Princeton Superpipe constants ($A_l = 4.3$ and $\kappa_l = 0.39$), $z_l^+ = 0.18$, see Fig. 1.

In the following, we will use the square of the log-law:

$$\frac{U_l^2(z)}{U_\tau^2} = \frac{1}{\kappa_l^2} \log^2(z^+) + A_l^2 + \frac{2A_l}{\kappa_l} \log(z^+). \tag{9}$$

According to the attached-eddy hypothesis prediction by Townsend,^{6,12} the streamwise fluctuating velocity u_l can be written as

$$\frac{\overline{u_l^2}(z)}{U_\tau^2} = B_{1,l} - A_{1,l} \log(z/\delta), \tag{10}$$

where $B_{1,l}$ and $A_{1,l}$ are constants. For the Princeton Superpipe, we use $B_{1,l} = 1.56$ and $A_{1,l} = 1.26$, see Fig. 2. We use $A_{1,l} = 1.26$, which is an average of several datasets, including Superpipe measurements. The fit to Superpipe measurements gave $A_{1,l} = 1.23 \pm 0.05$.⁶

We use Eqs. (9) and (10) to define the square of the turbulence intensity (TI),

$$I_l^2(z) |_{\text{log-law}} = \frac{\overline{u_l^2}(z)}{U_l^2(z)} = \frac{B_{1,l} - A_{1,l} \log(z/\delta)}{\frac{1}{\kappa_l^2} \log^2(z^+) + A_l^2 + \frac{2A_l}{\kappa_l} \log(z^+)}. \tag{11}$$

Here, the two terms in the numerator are both positive and equal if z/δ is

$$z/\delta |_{0,l} = \exp(-B_{1,l}/A_{1,l}). \tag{12}$$

For the Superpipe constants, $z/\delta |_{0,l} = 0.29$, see Fig. 3; the measured near-wall low Re_τ I^2 from Ref. 13 is shown as a horizontal line for reference. We observe that the TI decreases with increasing Re_τ .

For the Princeton Superpipe measurements, Re_τ ranges from 1985 to 98 190; the logarithm of these numbers is 7.6 and 11.5, respectively.

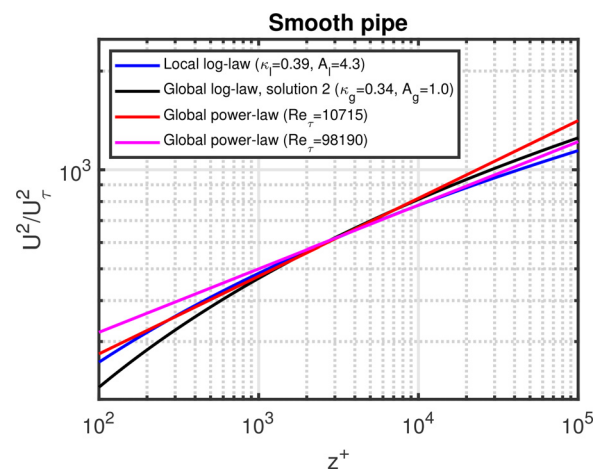


FIG. 1. Square of the normalized mean velocity as a function of z^+ . The blue line shows Eq. (9). The other lines are defined and referred to later in this paper: Secs. IV C 1 and IV C 2.

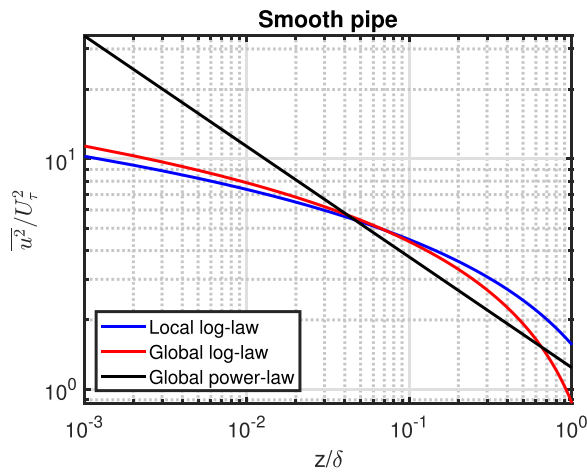


FIG. 2. Square of the normalized fluctuating velocity as a function of z/δ . The blue line shows Eq. (10). The other lines are defined and referred to later in this paper: Secs. IV B 1 and IV B 2.

IV. GLOBAL SCALING

A. Radial averaging definitions

In this paper, we make use of two radial averaging definitions, arithmetic mean (AM) and area-averaged (AA). The reason for employing two methods is to extract two averages from the same measurements. This in turn allows us to construct radial profiles of the squared normalized fluctuating and mean velocities with two parameters. The result is two equations with two unknowns, i.e., the two profile parameters.

1. Arithmetic mean

The arithmetic mean (AM) is defined as

$$\langle \cdot \rangle_{AM} = \frac{1}{\delta} \int_0^\delta [\cdot] dz \tag{13}$$

$$= \frac{1}{Re_\tau} \int_0^{Re_\tau} [\cdot] dz^+, \tag{14}$$

where we define the average both integrating over z and z^+ .

2. Area-averaged

The area-average (AA) is defined as

$$\langle \cdot \rangle_{AA} = \frac{2}{\delta^2} \int_0^\delta [\cdot] \times (\delta - z) dz \tag{15}$$

$$= \frac{2}{Re_\tau} \int_0^{Re_\tau} [\cdot] dz^+ - \frac{2}{Re_\tau^2} \int_0^{Re_\tau} [\cdot] \times z^+ dz^+. \tag{16}$$

B. Velocity fluctuations

The averaged square of the measured normalized fluctuating velocities is shown in Fig. 4, both for smooth- and rough-wall pipe flow. Both the AM and AA averaging is shown; they have different amplitude, but both averages are roughly constant as a function of Reynolds number. We also note that the smooth- and rough-wall results are comparable.

In general, we show both smooth- and rough-wall measurements, but only use the smooth-wall measurements for postprocessing. The rough-wall measurements are shown for reference and to indicate whether they follow the smooth-wall behavior or not.

1. Log-law

The AM average of the log-law for the fluctuating velocity, Eq. (10), has been derived in Ref. 14,

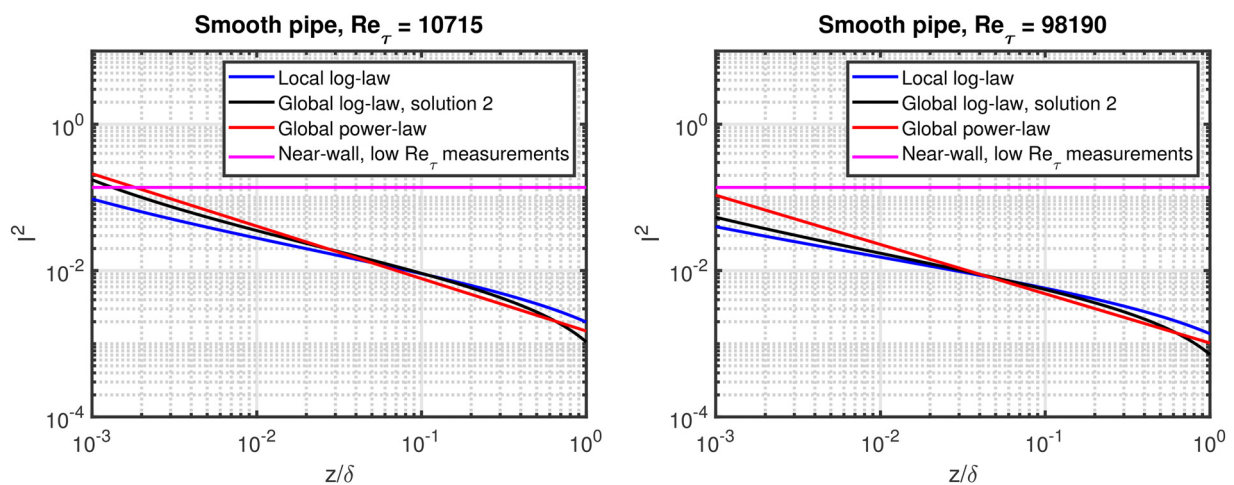


FIG. 3. \bar{u}'^2 as a function of z/δ . Left: $Re_\tau = 10715$, right: $Re_\tau = 98190$. The blue lines show Eq. (11). The magenta lines show the value $(0.37)^2$ which has been measured in the vicinity of the wall for low Re_τ turbulent pipe flow.¹³ The other lines are defined and referred to later in this paper: Sec. V D.

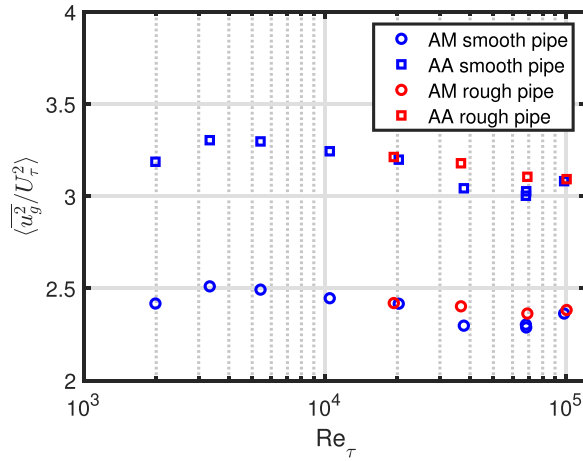


FIG. 4. The averaged square of the measured normalized fluctuating velocities as a function of Reynolds number.

$$\begin{aligned} \left\langle \frac{\overline{u_g^2}}{U_\tau^2} \right\rangle_{AM, \log-law} &= \frac{1}{\delta} \int_0^\delta [B_{1,g} - A_{1,g} \log(z/\delta)] dz & (17) \\ &= B_{1,g} + A_{1,g}, & (18) \end{aligned}$$

where the subscript “g” means that the parameters are “global,” i.e., covering the entire range of z.

The corresponding AA average has been derived in Ref. 2,

$$\begin{aligned} \left\langle \frac{\overline{u_g^2}}{U_\tau^2} \right\rangle_{AA, \log-law} &= \frac{2}{\delta^2} \int_0^\delta [B_{1,g} - A_{1,g} \log(z/\delta)] \times (\delta - z) dz & (19) \\ &= B_{1,g} + \frac{3}{2} \times A_{1,g}, & (20) \end{aligned}$$

the difference being a factor 3/2 multiplied with $A_{1,g}$.

For each Reynolds number, the two averages can be used along with the measurements in Fig. 4 to derive $A_{1,g}$ and $B_{1,g}$, see Fig. 5. The mean and standard deviation is

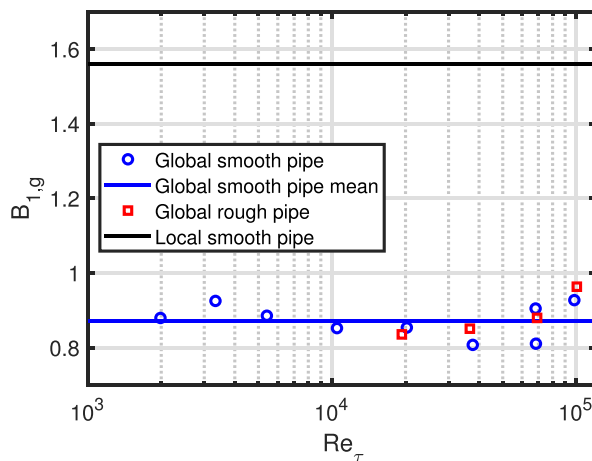
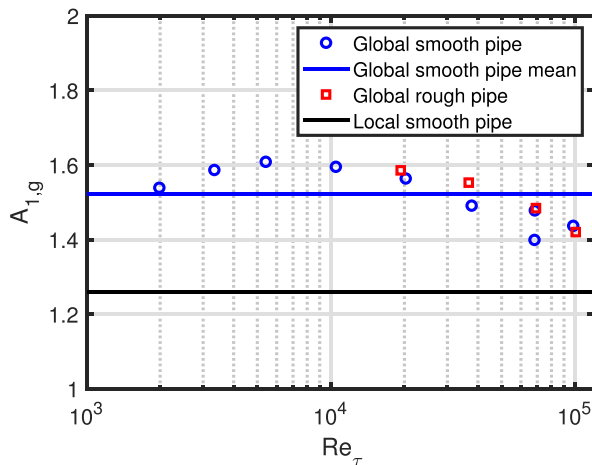


FIG. 5. Left-hand plot: $A_{1,g}$ vs Re_τ , right-hand plot: $B_{1,g}$ vs Re_τ . The smooth-wall average is shown as blue lines and the local parameter value as black lines.

$$A_{1,g} = 1.52 \pm 0.07, \tag{21}$$

$$B_{1,g} = 0.87 \pm 0.04, \tag{22}$$

compared to $A_{1,l} = 1.26$ and $B_{1,l} = 1.56$ for the local parameters. The global parameters can be used to calculate the AM and AA averages,

$$\left\langle \frac{\overline{u_g^2}}{U_\tau^2} \right\rangle_{AM, \log-law} = 2.39 \pm 0.08, \tag{23}$$

$$\left\langle \frac{\overline{u_g^2}}{U_\tau^2} \right\rangle_{AA, \log-law} = 3.15 \pm 0.09, \tag{24}$$

where we have propagated the errors from Eqs. (21) and (22). The relative error for both the AM and AA averages is 3%, which is comparable to the 3.4% uncertainty of the Princeton Superpipe measurements, see Table II in Ref. 4.

Results using the global parameters are shown in Fig. 2 as the “global log-law.”

2. Power-law

In addition to the log-law for the fluctuating velocity, our alternative radial profile will be a power-law function which we write introducing two new parameters a_g and b_g ,

$$\frac{\overline{u_g^2}(z)}{U_\tau^2} = a_g \times \left(\frac{z}{\delta}\right)^{b_g}. \tag{25}$$

As we did for the log-law, we calculate the AM and AA averages of this function,

$$\left\langle \frac{\overline{u_g^2}}{U_\tau^2} \right\rangle_{AM, power-law} = \frac{1}{\delta} \int_0^\delta \left[a_g \times \left(\frac{z}{\delta}\right)^{b_g} \right] dz \tag{26}$$

$$= \frac{a_g}{b_g + 1}, \tag{27}$$

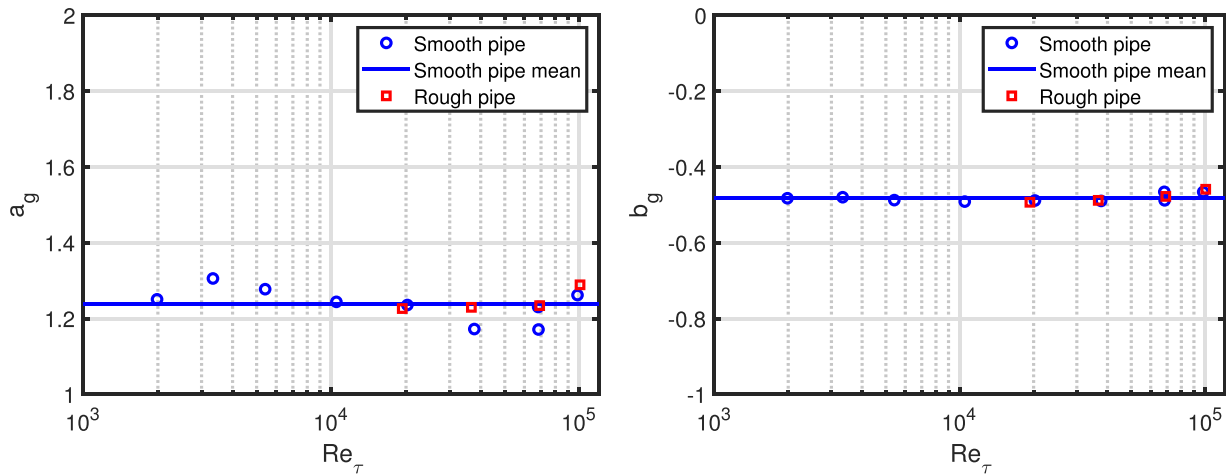


FIG. 6. Left-hand plot: a_g vs Re_τ , right-hand plot: b_g vs Re_τ . The smooth-wall average is shown as blue lines.

$$\left\langle \frac{u_g^2}{U_\tau^2} \right\rangle_{AA, power-law} = \frac{2}{\delta^2} \int_0^\delta \left[a_g \times \left(\frac{z}{\delta} \right)^{b_g} \right] \times (\delta - z) dz \quad (28)$$

$$= \frac{2a_g}{(b_g + 1)(b_g + 2)}. \quad (29)$$

As for the log-law, these two averaged equations can be used with the measurements in Fig. 4 to calculate a_g and b_g for each Reynolds number, see Fig. 6.

The mean and standard deviation using the smooth-wall measurements is

$$a_g = 1.24 \pm 0.04, \quad (30)$$

$$b_g = -0.48 \pm 0.01. \quad (31)$$

By construction, the global power-law parameters yield (almost) the same result for the AM and AA averages as the global log-law parameters,

$$\left\langle \frac{u_g^2}{U_\tau^2} \right\rangle_{AM, power-law} = 2.38, \quad (32)$$

$$\left\langle \frac{u_g^2}{U_\tau^2} \right\rangle_{AA, power-law} = 3.14. \quad (33)$$

Results using the global power-law parameters are shown in Fig. 2 as the “global power-law.” The shape of the power-law is very different from the log-law profiles, also in the range where the log-law matches measurements well. This is an indication that the power-law is far from reality; in that sense, it is a mathematical abstraction. However, the average of the profile does match the average of the measurements as is the case for the log-law.

C. Mean velocity

The averaged square of the measured normalized mean velocities is shown in Fig. 7, both for smooth- and rough-wall pipe flow. Both the AM and AA averaging is shown; they increase with Reynolds number, but opposed to the fluctuating velocity, the amplitude of the AM averaging is higher than that for the AA averaging. We can thus already

conclude that the scaling of the TI is really due to the scaling of the mean velocity. For this case, the smooth- and rough-wall results deviate.

1. Log-law

As we did for the fluctuating velocities, we also average the square of the mean velocities. The AM average of the log-law has been derived in Ref. 15,

$$\left\langle \frac{U_g^2}{U_\tau^2} \right\rangle_{AM, log-law} = \frac{1}{Re_\tau} \int_0^{Re_\tau} \left[\frac{1}{\kappa_g} \log(z^+) + A_g \right]^2 dz^+ \quad (34)$$

$$= \frac{2}{\kappa_g^2} - \frac{2A_g}{\kappa_g} + A_g^2 + \log(Re_\tau) \left(\frac{2A_g}{\kappa_g} - \frac{2}{\kappa_g^2} \right) + \frac{\log^2(Re_\tau)}{\kappa_g^2}, \quad (35)$$

and the AA average is

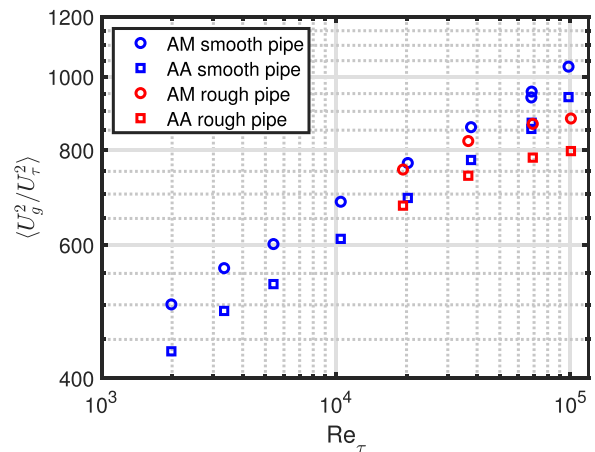


FIG. 7. The averaged square of the measured normalized mean velocities as a function of Reynolds number.

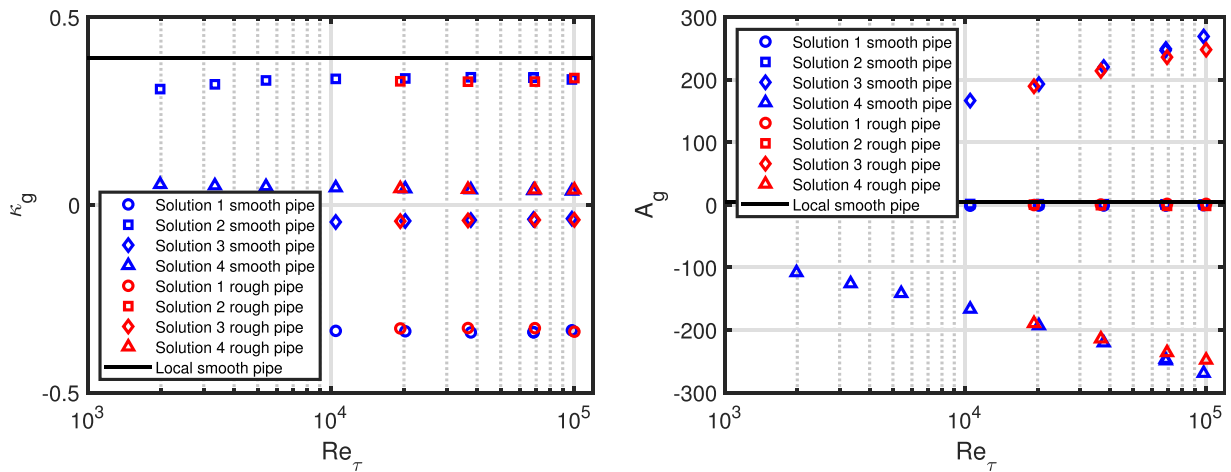


FIG. 8. Left-hand plot: κ_g as a function of Re_τ , right-hand plot: A_g as a function of Re_τ . The local parameter values are shown as black lines.

$$\begin{aligned}
 \left\langle \frac{U_g^2}{U_\tau^2} \right\rangle_{AA, \log\text{-law}} &= \frac{2}{Re_\tau} \int_0^{Re_\tau} \left[\frac{1}{\kappa_g} \log(z^+) + A_g \right]^2 dz^+ \\
 &\quad - \frac{2}{Re_\tau^2} \int_0^{Re_\tau} \left[\frac{1}{\kappa_g} \log(z^+) + A_g \right]^2 \times z^+ dz^+ \quad (36) \\
 &= \frac{7}{2\kappa_g^2} - \frac{3A_g}{\kappa_g} + A_g^2 + \log(Re_\tau) \left(\frac{2A_g}{\kappa_g} - \frac{3}{\kappa_g^2} \right) \\
 &\quad + \frac{\log^2(Re_\tau)}{\kappa_g^2}. \quad (37)
 \end{aligned}$$

These two equations along with the averaged measurements form a system of two quadratic equations; thus, we have four solutions; κ_g and A_g for these solutions are shown in Fig. 8. Only two of the solutions are unique; the other two are mirror images, see Fig. 9. Note that we show the normalized mean velocity; the square of this yields two unique solutions.

We focus on solution 2, which is the solution where κ_g and A_g are closest to κ_l and A_l . $A_{g, \text{solution 2}}$ does not vary with Re_τ , whereas $\kappa_{g, \text{solution 2}}$ does,

$$A_{g, \text{solution 2}} = 1.01 \pm 0.32, \quad (38)$$

$$\kappa_{g, \text{solution 2}} = 0.34 - 623.9 \times Re_\tau^{-1.31}, \quad R^2 = 0.97. \quad (39)$$

Solution 2 is provided as mean and standard deviation for $A_{g, \text{solution 2}}$ and as a function of Re_τ for $\kappa_{g, \text{solution 2}}$ along with the coefficient of determination R^2 . Values are shown in Fig. 10. The asymptotic value for $\kappa_{g, \text{solution 2}}$ is 0.34; this solution is shown as the “global log-law, solution 2” in Fig. 1. The rough-wall pipe parameters deviate from the smooth-wall pipe results.

We define a Re_τ threshold from the $\kappa_{g, \text{solution 2}}$ scaling which we determine as the value where 99% of the asymptotic value of $\kappa_{g, \text{solution 2}}$ is reached. This threshold value is $Re_\tau|_{\text{threshold}} = 10715$, see the vertical magenta line in the left-hand plot of Fig. 10. This

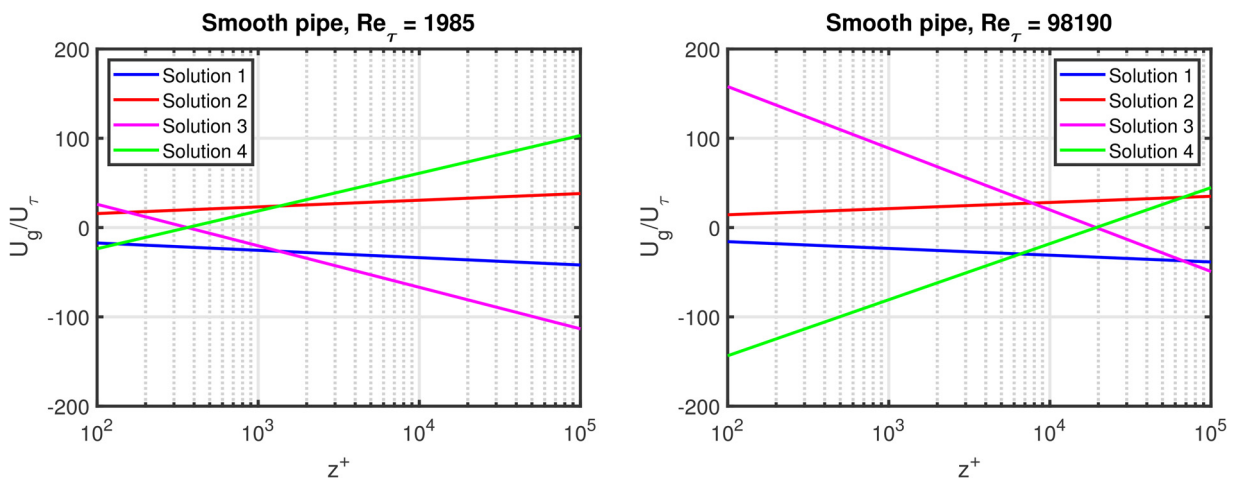


FIG. 9. Normalized mean velocity as a function of z^+ for the four solutions. Left-hand plot: $Re_\tau = 1985$, right-hand plot: $Re_\tau = 98190$.

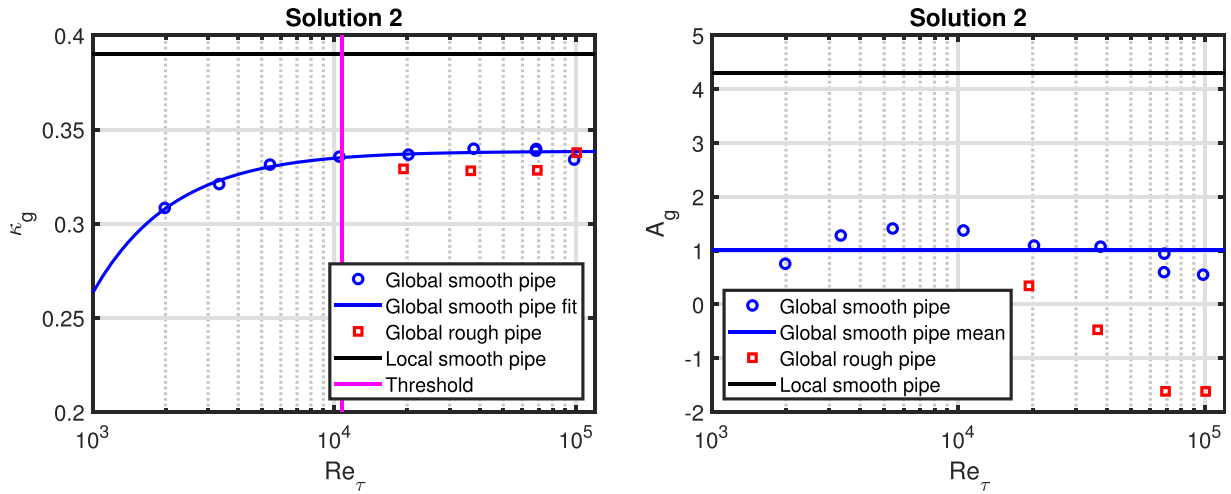


FIG. 10. Left-hand plot: $\kappa_{g,solution\ 2}$ vs Re_τ , right-hand plot: $A_{g,solution\ 2}$ vs Re_τ . Blue lines are Eqs. (38) and (39), and local parameter values are black lines.

establishes a high Reynolds number transition region which will be a recurring topic in the remainder of this paper.

Solution 4, which has a small positive κ_g and a large negative A_g , will be treated in the Discussion. It is a solution which has the zero crossing at much larger values of z^+ than solution 2 because of a large amplitude (but negative) $\kappa_g A_g$ product.

The difference between Eqs. (35) and (37) is

$$\left\langle \frac{U_g^2}{U_\tau^2} \right\rangle_{AM, \log-law} - \left\langle \frac{U_g^2}{U_\tau^2} \right\rangle_{AA, \log-law} = \frac{A_g}{\kappa_g} - \frac{3}{2\kappa_g^2} + \log(Re_\tau) \left(\frac{1}{\kappa_g^2} \right), \tag{40}$$

which is shown for $A_g = 1.01$ [Eq. (38)] and $\kappa_g = 0.34$ [Eq. (39)] in Fig. 11 along with the difference for the measurements. As expected, the difference scales with $\log(Re_\tau)$ for Reynolds numbers above the threshold.

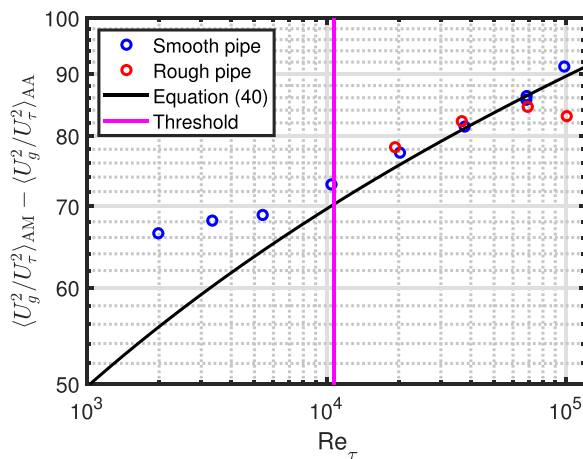


FIG. 11. $\left\langle \frac{U_g^2}{U_\tau^2} \right\rangle_{AM} - \left\langle \frac{U_g^2}{U_\tau^2} \right\rangle_{AA}$ vs Re_τ , the black line is Eq. (40).

2. Power-law

For the mean velocity, we also identify an alternative radial power-law profile with two new parameters c_g and d_g for the squared normalized mean velocity,

$$\frac{U_g^2(z)}{U_\tau^2} = c_g \times (z^+)^{d_g}. \tag{41}$$

The AM and AA averages of Eq. (41) are

$$\left\langle \frac{U_g^2}{U_\tau^2} \right\rangle_{AM, power-law} = \frac{1}{Re_\tau} \int_0^{Re_\tau} [c_g \times (z^+)^{d_g}] dz^+ \tag{42}$$

$$= \frac{c_g}{d_g + 1} \times Re_\tau^{d_g}, \tag{43}$$

$$\left\langle \frac{U_g^2}{U_\tau^2} \right\rangle_{AA, power-law} = \frac{2}{Re_\tau} \int_0^{Re_\tau} [c_g \times (z^+)^{d_g}] dz^+ - \frac{2}{Re_\tau^2} \int_0^{Re_\tau} [c_g \times (z^+)^{d_g}] \times z^+ dz^+ \tag{44}$$

$$= \frac{2c_g}{(d_g + 1)(d_g + 2)} \times Re_\tau^{d_g}. \tag{45}$$

From solving the equations, it is clear that both c_g and d_g have a Reynolds number dependency, see Fig. 12. The rough-wall data differ from the smooth-wall solutions for the power-law profile as it did for the log-law.

We fit the parameters to power-laws of Re_τ above $Re_\tau|_{threshold}$,

$$c_g = c_1 \times Re_\tau^{c_2} \tag{46}$$

$$= 21.25 \times Re_\tau^{0.16}, \quad R^2 = 0.97, \tag{47}$$

$$d_g = d_1 \times Re_\tau^{d_2} \tag{48}$$

$$= 0.55 \times Re_\tau^{-0.09}, \quad R^2 = 0.99. \tag{49}$$

The solution is shown for $Re_\tau = 10\ 715$ and $Re_\tau = 98\ 190$ as the “global power-law” in Fig. 1.

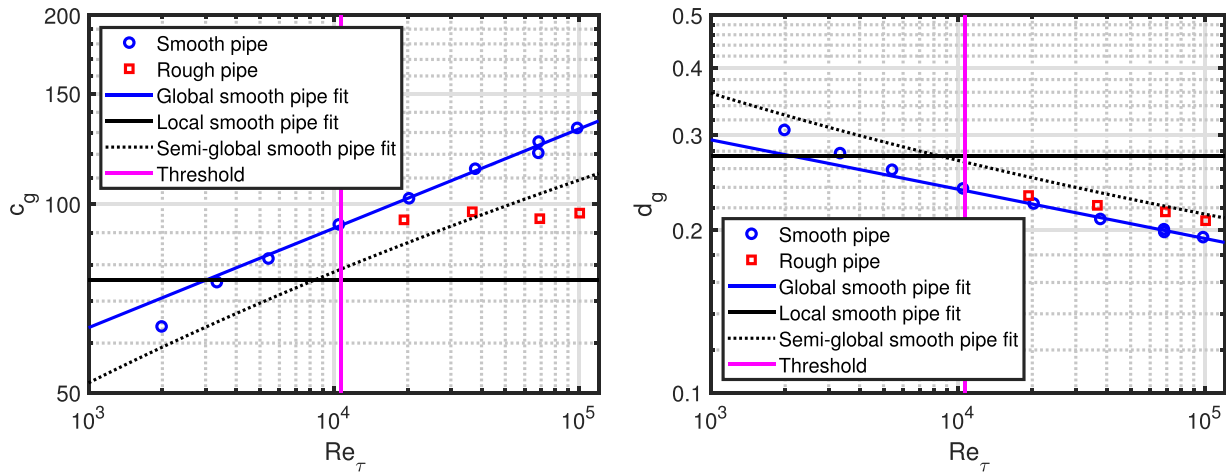


FIG. 12. Left-hand plot: c_g as function of Re_τ , right-hand plot: d_g as function of Re_τ . Blue lines are Eqs. (47) and (49), black solid lines are local values from Eq. (50), and black dotted lines are semi-global values from Eq. (51).

Also included in Fig. 12 are previous results for local and semi-global (subscript “s-g”) power-law fits to Superpipe measurements,^{16,17}

$$\frac{U_1^2(z)}{U_\tau^2} = [8.70 \times (z^+)^{0.137}]^2, \tag{50}$$

$$\frac{U_{s-g}^2(z)}{U_\tau^2} = \left[(0.7053 \times \log(Re_D) + 0.3055) \times (z^+)^{\frac{1.085}{\log(Re_D)} + \frac{6.535}{\log^2(Re_D)}} \right]^2, \tag{51}$$

where $Re_D = D\langle U_g \rangle_{AA}/\nu$ is the bulk Reynolds number based on the pipe diameter $D = 2R$. We use an equation derived in Ref. 3 to convert between Re_τ and Re_D ,

$$Re_\tau = 0.0621 \times Re_D^{0.9148}. \tag{52}$$

Note that the exponent in Eq. (52) is found to be 12/13 = 0.923 1 in Ref. 18, which deviates less than 1% from our result.

The local power-law fit was done for $60 < z^+ < 0.15Re_\tau$ and the semi-global power-law fit covered a range $40 < z^+ < 0.85Re_\tau$. The local power-law fit can be compared to a range of $3\sqrt{Re_\tau} < z^+ < 15Re_\tau$ used for the local log-law fits in Ref. 6.

As mentioned in Ref. 16, the local power-law exponent in Eq. (50), 0.137, is close to the 1/7 exponent (“the 1/7th law”) proposed by von Kármán and Prandtl as a global power-law for the low Reynolds number mean velocity (see chapter 2.4 in Ref. 19 for the historical context).

It is interesting to note that the semi-global and global power-law parameters scale with Re_τ in a similar fashion; the difference is mainly an offset, which is due to the different radial ranges used for the fits.

V. DISCUSSION

A. The high Reynolds number transition placed in context

As stated, we have identified a transition in mean flow behavior around $Re_\tau|_{\text{threshold}} = 10715$ at the point where $\kappa_{g,\text{solution 2}}$ reached

99% of the asymptotic value. This criterion is of course arbitrary to some extent; if we instead require 95%, the transitional Re_τ is 3126, a factor of three lower, see Fig. 13. Therefore, a single transitional Reynolds number is difficult to pin down, indicating that there is a gradual rather than an abrupt transition.

The transition we have found in this paper is consistent with earlier indications of transition, see Appendix D in Ref. 1.

In Ref. 20, it is shown that the turbulent kinetic energy production in the logarithmic region exceeds the near-wall production above $Re_\tau \approx 4200$. This could be linked to the transition we are describing in this paper.

Global averaging has previously been used in Ref. 21, where the streamwise component of the area-averaged mean turbulent kinetic energy is calculated,

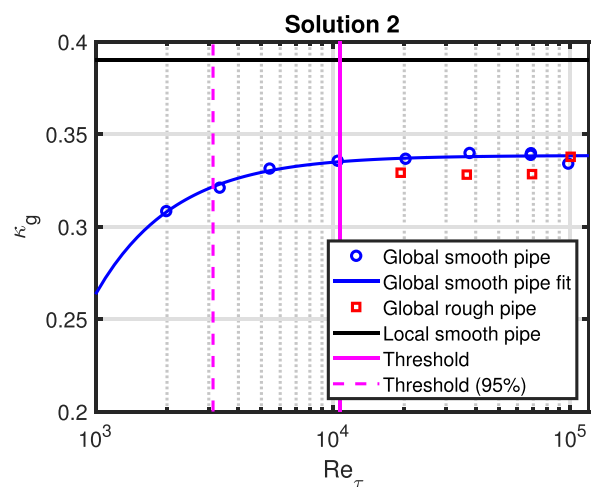


FIG. 13. $\kappa_{g,\text{solution 2}}$ vs Re_τ . The transitional Re_τ using the 99% (95%) criterion is shown as the vertical solid (dashed) magenta line, respectively.

$$K = \left\langle \frac{u^2}{2} \right\rangle_{AA}, \tag{53}$$

which can be related to the area-average of the square of the normalized fluctuating velocity used in this paper,

$$\left\langle \frac{u_g^2}{U_\tau^2} \right\rangle_{AA} = \frac{2K}{U_\tau^2}. \tag{54}$$

As a consistency check, we can compare results for K/U_τ^2 in Ref. 21 with values we have calculated: They find that the ratio is in the range 1.6–1.7 above $Re_D \approx 10^5$. Multiplying this by two to convert to $\langle u_g^2/U_\tau^2 \rangle_{AA}$, we find a range 3.2–3.4 which agrees fairly well with the average value of the Superpipe measurements, namely, 3.2, see Fig. 4 and Eqs. (24) and (33).

A transition in the friction factor from Blasius scaling to “extreme-Re” scaling has been identified for smooth pipes in Ref. 18,

$$\lambda_{\text{Blasius}} = \frac{3.16 \times 10^{-1}}{Re_D^{1/4}}, \tag{55}$$

$$\lambda_{\text{Extreme-Re}} = \frac{9.946 \times 10^{-2}}{Re_D^{2/13}}, \tag{56}$$

see Fig. 14. The nominal value for the transition is $Re_D = 166\,418$. A universal model for the friction factor in smooth pipes has been published in Ref. 22.

Under certain assumptions, the Blasius friction factor scaling can be used to derive the global 1/7th law, see division G, Sec. 22 in Ref. 23,

$$\frac{U_{g-\text{Blasius}}^2(z)}{U_\tau^2} = \left[8.74 \times (z^+)^{1/7} \right]^2. \tag{57}$$

Results from Refs. 18, 20, 21, and 24, and this paper are summarized in Table I. For all cases, both Re_τ and Re_D are shown. The results agree within a factor of two except for Ref. 24 and the “threshold (99%)” values which are roughly a factor of three

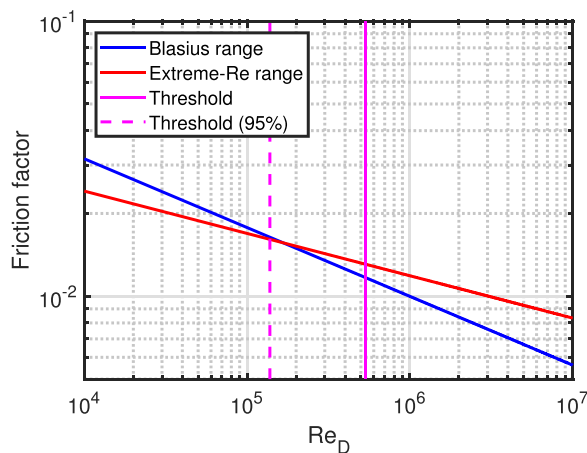


FIG. 14. Friction factor as a function of Re_D for smooth pipes. The transitional Re_D using the 99% (95%) criterion is shown as the vertical solid (dashed) magenta line, respectively.

TABLE I. Transition Reynolds number.

Source	Re_τ	Re_D
Marusic <i>et al.</i> ²⁰	4200	1.9×10^5
Yakhot <i>et al.</i> ²¹	2329	1.0×10^5
Anbarlooei <i>et al.</i> ¹⁸	3711	1.7×10^5
Skouloudis and Hwang ²⁴	10^4	4.9×10^5
Threshold (95%)	3126	1.4×10^5
Threshold (99%)	10 715	5.3×10^5

higher. It seems likely that all results detect the same transition; however, from our analysis it appears that the transitional Reynolds number is higher than the previously estimated one, but consistent with Ref. 24.

B. On the properties of the von Kármán constant

A theory has been proposed where $z + z_{\text{offset}}$ is considered instead of z , z_{offset} being an offset associated with a mesolayer.²⁵ One consequence is the variation of the von Kármán constant with Reynolds number,

$$\kappa_{\text{offset}} = \frac{\kappa_\infty (\log(D_s Re_\tau))^{1+\alpha}}{(\log(D_s Re_\tau))^{1+\alpha} - \alpha A \kappa_\infty}, \tag{58}$$

which is shown in the left-hand plot of Fig. 15 for $\kappa_\infty = 0.447$, $D_s = 1$, $\alpha = 0.44$, and $A = -0.67$. The trend is similar to what we have observed, but the approach to the asymptotic value of the von Kármán constant is slower for the offset theory, see the right-hand plot of Fig. 15.

Variations of the von Kármán constant with Reynolds number have been compared for different canonical flows in Ref. 26. The von Kármán constant approaches an asymptotic value, but the value of this number is different for the three flow types. These results and others are included in Ref. 27, and it is stated that the von Kármán constant approaches the asymptotic value from below for pipe flow, which matches what we have found.

The concepts of active and inactive vortex motion^{12,28} relates to effects of smaller near-wall and larger core eddies. In Ref. 29, a possible consequence of this distinction is shown to be scaling of the von Kármán constant with Reynolds number. The outcome is that the measured value of the von Kármán constant is larger than the universal value by a factor which depends on the streamwise TI squared among other terms.

C. Length scales

A characteristic mixing length scale l_m (see Chap. 2.5 in Ref. 19) can be found by differentiating the mean velocity log-law,

$$\frac{dU^+}{dz} = \frac{1}{\kappa z} = \frac{1}{l_m}, \tag{59}$$

which shows that the scale of turbulence is proportional to the distance from the wall (attached eddies¹²),

$$l_m = \kappa z. \tag{60}$$

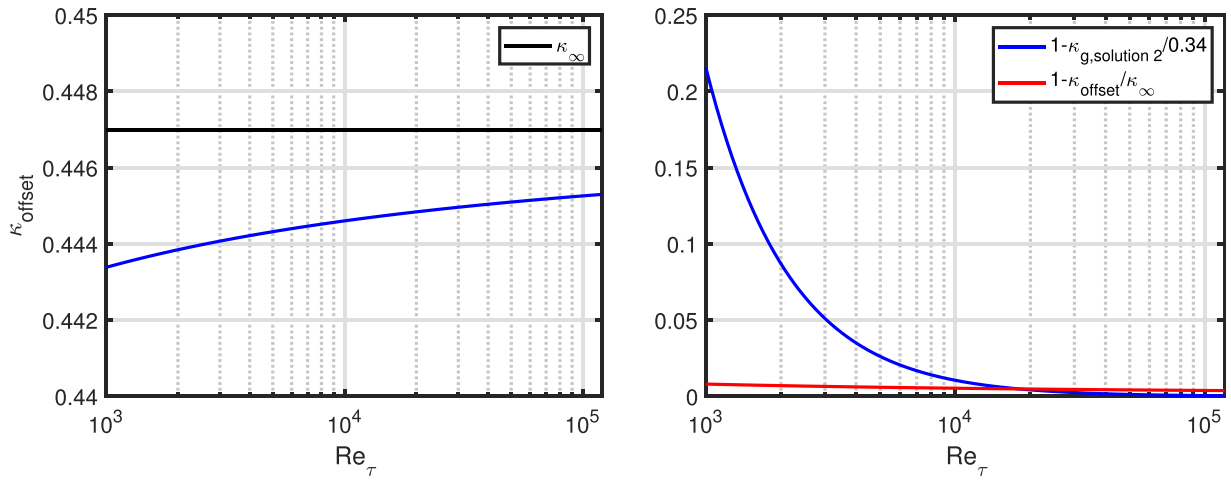


FIG. 15. Left-hand plot: κ_{offset} vs Re_τ , right-hand plot: Comparison between normalized change of $\kappa_{g,\text{solution 2}}$ and κ_{offset} .

Since we have found that $\kappa_g < \kappa_l$, the global characteristic length scale $l_g = \kappa_g z$ is smaller than the corresponding local length scale $l_l = \kappa_l z$ for a given distance from the wall. We also note that if the von Kármán constant increases with Reynolds number, the turbulent structure size increases correspondingly.

Integral length scales can be found by calculating the AM and AA of the mixing length,

$$l_{i,AM} = \langle l_m \rangle_{AM} = \frac{1}{\delta} \times \int_0^\delta \kappa z dz = \frac{\kappa \delta}{2}, \quad (61)$$

$$l_{i,AA} = \langle l_m \rangle_{AA} = \frac{2}{\delta^2} \times \int_0^\delta \kappa z \times (\delta - z) dz = \frac{\kappa \delta}{3}. \quad (62)$$

In Ref. 30, a turbulent length scale is derived from the normalized correlation function $R(z)$ to be

$$l_c = \int_0^\delta R(z) dz \approx 0.14 \delta. \quad (63)$$

If we require $l_{i,AM} = l_c$ ($l_{i,AA} = l_c$), we get $\kappa = 0.28$ (0.42), respectively, which is comparable to the range of values between κ_g and κ_l .

Our discussion pertains to wall-normal length scales; spanwise and/or streamwise structures can extend to lengths far greater than the pipe diameter.

D. Radial profiles of turbulence intensity

The global log-law TI profile is defined as in Eq. (11), but with the subscript changed from “l” to “g.” This is shown for solution 2 as “global log-law, solution 2” in Fig. 3. In this figure, the “global power-law” is also present, defined as

$$I_g^2(z) |_{\text{power-law}} = \frac{a_g \times \left(\frac{z}{\delta}\right)^{b_g}}{c_g \times (z^+)^{d_g}}. \quad (64)$$

E. Turbulence intensity scaling with Reynolds number

Below we define the TI squared using ratios for either log- or power-laws separately.

The averaged global TI squared is defined below for AM and AA, see Fig. 16,

$$\langle I_g^2 \rangle_{AM} = \left\langle \frac{\overline{u_g^2}}{U_\tau^2} \right\rangle_{AM} / \left\langle \frac{U_g^2}{U_\tau^2} \right\rangle_{AM}, \quad (65)$$

$$\langle I_g^2 \rangle_{AA} = \left\langle \frac{\overline{u_g^2}}{U_\tau^2} \right\rangle_{AA} / \left\langle \frac{U_g^2}{U_\tau^2} \right\rangle_{AA}. \quad (66)$$

1. Log-law

The averaged global TI squared for the log-law is defined for AM using Eqs. (18) and (35),

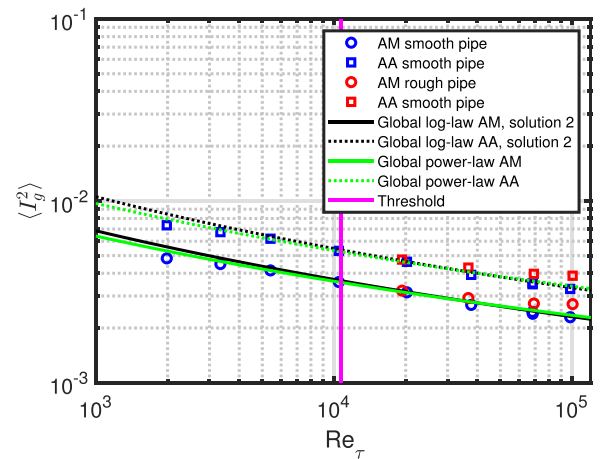


FIG. 16. Averaged global TI squared as a function of Re_τ .

$$\langle I_g^2 \rangle_{AM, \log-law} = \frac{B_{1,g} + A_{1,g}}{\frac{2}{\kappa_g^2} - \frac{2A_g}{\kappa_g} + A_g^2 + \log(Re_\tau) \left(\frac{2A_g}{\kappa_g} - \frac{2}{\kappa_g^2} \right) + \frac{\log^2(Re_\tau)}{\kappa_g^2}} \quad (67)$$

The averaged global TI squared for the log-law is defined for AA using Eqs. (20) and (37),

$$\langle I_g^2 \rangle_{AA, \log-law} = \frac{B_{1,g} + \frac{3}{2} \times A_{1,g}}{\frac{7}{2\kappa_g^2} - \frac{3A_g}{\kappa_g} + A_g^2 + \log(Re_\tau) \left(\frac{2A_g}{\kappa_g} - \frac{3}{\kappa_g^2} \right) + \frac{\log^2(Re_\tau)}{\kappa_g^2}} \quad (68)$$

These definitions are shown as black lines in Fig. 16. Mean values of $A_{1,g}$ and $B_{1,g}$ from Eqs. (21) and (22) have been used.

2. Power-law

The averaged global TI squared for the power-law is defined for AM using Eqs. (27) and (43),

$$\langle I_g^2 \rangle_{AM, power-law} = \frac{a_g}{b_g + 1} \times \frac{d_g + 1}{c_g \times Re_\tau^{d_g}} \quad (69)$$

The averaged global TI squared for the power-law is defined for AA using Eqs. (29) and (45),

$$\langle I_g^2 \rangle_{AA, power-law} = \frac{2a_g}{(b_g + 1)(b_g + 2)} \times \frac{(d_g + 1)(d_g + 2)}{2c_g \times Re_\tau^{d_g}} \quad (70)$$

These definitions are shown as green lines in Fig. 16.

F. Turbulence intensity scaling with friction factor

We have presented results relating the TI and the friction factor in Refs. 2 and 3, and we can discuss it further based on our findings in this paper. The friction factor is defined as

$$\lambda = 8 \frac{U_\tau^2}{\langle U_g^2 \rangle_{AA}} = \frac{8}{\left\langle \frac{U_g^2}{U_\tau^2} \right\rangle_{AA}} \quad (71)$$

which can be rewritten as

$$\langle I_g^2 \rangle_{AA} = \frac{\lambda}{8} \times \left\langle \frac{u_g^2}{U_\tau^2} \right\rangle_{AA} \quad (72)$$

$$= \frac{\lambda}{8} \times \left(B_{1,g} + \frac{3}{2} \times A_{1,g} \right) \quad (73)$$

$$= \frac{\lambda}{8} \times \frac{2a_g}{(b_g + 1)(b_g + 2)} \quad (74)$$

$$= 0.39 \times \lambda \quad (75)$$

$$= \kappa_l \times \lambda, \quad (76)$$

leading to a simple relationship between the area-averaged, squared TI, and the friction factor in the final Eq. (76): They are proportional with the local von Kármán constant κ_l as the factor of proportionality.

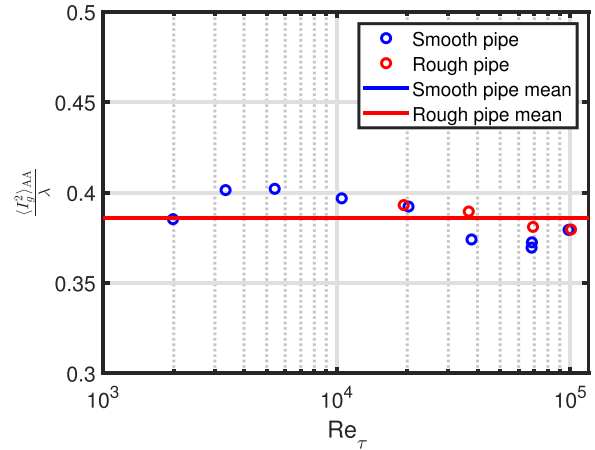


FIG. 17. $\langle I_g^2 \rangle_{AA}/\lambda$ as a function of Re_τ . The smooth- and rough-wall results are in the same range.

This relationship is illustrated in Fig. 17. It is generally valid, e.g., for all Re_τ and smooth- and rough-wall pipe flow.

We end by combining Eqs. (55) and (56) with Eq. (76) to derive expressions for the area-averaged, squared TI explicitly as a function of Re_D ,

$$\langle I_g^2 \rangle_{AA, Blasius} = \kappa_l \times \frac{3.16 \times 10^{-1}}{Re_D^{1/4}}, \quad (77)$$

$$\langle I_g^2 \rangle_{AA, Extreme-Re} = \kappa_l \times \frac{9.946 \times 10^{-2}}{Re_D^{2/13}} \quad (78)$$

The performance of these expressions is shown in Fig. 18. Note that the friction factor scaling used¹⁸ is for smooth pipes. The agreement with measurements is reasonable although the slope for the “extreme-Re” range is not matching the smooth pipe measurements exactly.

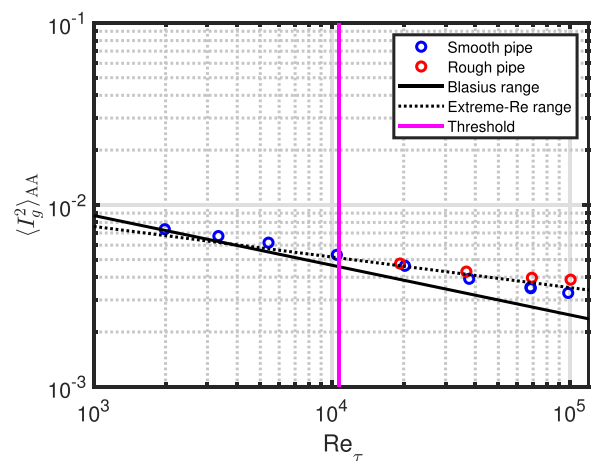


FIG. 18. $\langle I_g^2 \rangle_{AA}$ as a function of Re_τ . The solid (Blasius) and dotted (extreme-Re) lines are the smooth pipe predictions from Eqs. (77) and (78).

G. Alternative solutions to the global log-law

We have focused on solution 2 for the global mean velocity log-law. Here, we return briefly to the other solutions, see Fig. 9.

Solution 1 is simply flow in the reverse direction of solution 2.

Solutions 3 and 4 have zero crossings at much higher z^+ than the local log-law. If one would interpret this in a physical sense, it could be equivalent to Couette flow with walls moving in opposite directions, see e.g., Ref. 31.

For completeness, we characterize solution 4. Both $A_{g,solution 4}$ and $\kappa_{g,solution 4}$ are functions of Reynolds number. Fits for Reynolds numbers above the threshold yield

$$A_{g,solution 4} = -24.49 \times Re_\tau^{0.21}, \quad R^2 = 0.99, \quad (79)$$

$$\kappa_{g,solution 4} = 0.11 \times Re_\tau^{-0.10}, \quad R^2 = 0.99, \quad (80)$$

see Fig. 19. Thus, it adds some complexity compared to solution 2 where both parameters are constant above the threshold Reynolds number. However, it is a mathematically valid solution as well.

H. Higher order radial averaging

We have considered equations for fluctuating and mean velocities defined using two parameters. Thus, two equations for radial averaging were required, AM and AA.

If we were to consider, e.g., equations using three parameters, we would need a third radial averaging equation, volume averaging (VA).³

For this case, the square of the fluctuating and mean velocities could be expressed as

$$\frac{\overline{u_g^2}(z)}{U_\tau^2} = \alpha_g \times \left(\frac{z}{\delta}\right)^{\beta_g} + \gamma_g \quad (81)$$

and

$$\frac{U_g^2(z)}{U_\tau^2} = \varepsilon_g \times (z^+)^{\zeta_g} + \eta_g, \quad (82)$$

respectively, where $\alpha_g, \beta_g, \gamma_g, \varepsilon_g, \zeta_g,$ and η_g are parameters.

Other power- and log-law solutions, inspired by the offset solution²⁵ and grid-generated turbulence decay (see, e.g., Chap. 3.3.1 in Ref. 19), could be

$$\frac{\overline{u_g^2}(z)}{U_\tau^2} = \alpha_g \times \left(\frac{z}{\delta} + \gamma_g\right)^{\beta_g}, \quad (83)$$

$$\frac{U_g^2(z)}{U_\tau^2} = \varepsilon_g \times (z^+ + \eta_g)^{\zeta_g}, \quad (84)$$

$$\frac{\overline{u_g^2}(z)}{U_\tau^2} = \alpha_g - \beta_g \times \log\left(\frac{z}{\delta} + \gamma_g\right), \quad (85)$$

$$\frac{U_g^2(z)}{U_\tau^2} = (\zeta_g \times \log(z^+ + \eta_g) + \varepsilon_g)^2. \quad (86)$$

This is outside the scope of the current paper but will be addressed in future research.

I. Scaling of the peak of the squared normalized fluctuating velocity

We note that a radial redistribution of the velocity fluctuations as a function of Re_τ might occur—but not be detected—due to the averaging process.

We know that the peak of the squared normalized fluctuating velocity scales with Re_τ , but recent work^{32,33} indicates that the peak becomes asymptotically constant (bounded). This is in contrast to previous scaling expressions where the peak is proportional to the logarithm of the Reynolds number,³⁴ see Fig. 20. Using the expression for $\overline{u^2}/U_\tau^2|_{\text{peak}}$ in Ref. 32, the peak value is 9.6 for $Re_\tau = 10715$, which is 20% below the asymptotic value of 11.5. The Princeton Superpipe data we treat is part of the measurement database used in Ref. 32; it is interesting to note that the Superpipe peak values appear to become asymptotic at a value of roughly 9 for Re_τ above 4000. This value matches the transitional Reynolds numbers in Table I quite well.

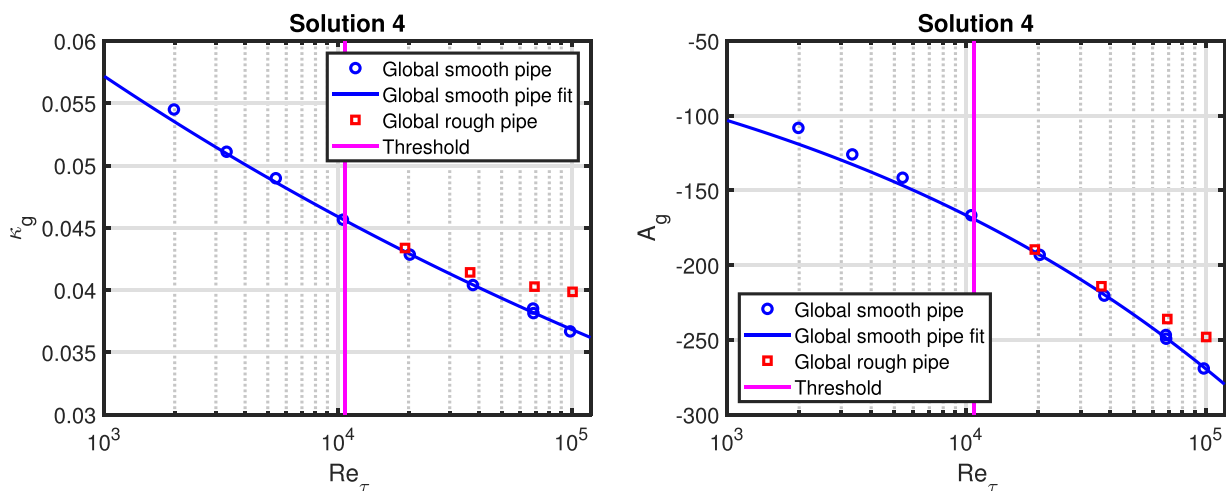


FIG. 19. Left-hand plot: $\kappa_{g,solution 4}$ vs Re_τ , right-hand plot: $A_{g,solution 4}$ vs Re_τ . Blue lines are Eqs. (79) and (80).

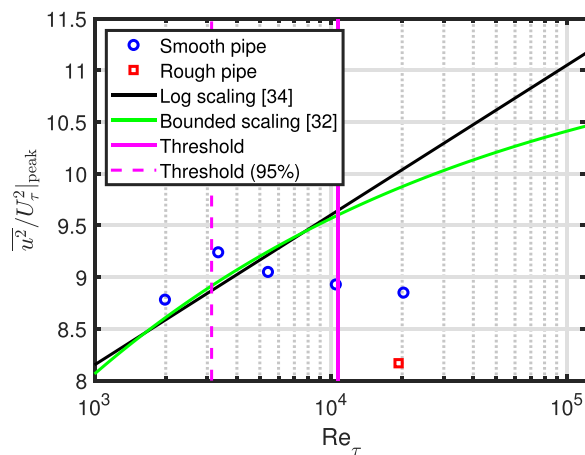


FIG. 20. $\overline{u^2}/U_\tau^2|_{\text{peak}}$ as a function of Re_τ . The solid black line is from Ref. 34 and the solid green line from Ref. 32. The transitional Re_τ using the 99% (95%) criterion is shown as the vertical solid (dashed) magenta line, respectively. Superpipe measurements are included for the Reynolds numbers where a distinct inner peak is visible.

J. Recommendations

As stated in Ref. 35, the log-law has the advantage over the power-law of being universal, i.e., independent of Reynolds number for asymptotically high Reynolds numbers.

The question of log- vs power-law behavior has been debated for more than a century, with bursts of publications followed by periods of relative calm. One such burst occurred in relation to the publication of Refs. 36 and 37, where a power-law approach was advocated, followed by various rebuttals, e.g., Ref. 16.

We have seen that log- and power-laws characterize the Superpipe measurements equally well, but the universality of the log-laws puts them at a slight advantage. To quote Ref. 29, “Occam’s razor might lead us to favor the log-law.”

VI. CONCLUSIONS

By an analysis of global properties of fluctuating and mean pipe flow velocities, we have characterized a high Reynolds number transition region at a friction Reynolds number $Re_\tau \sim 11\,000$. The transitional Reynolds number appears slightly higher than that reported in literature, so the global von Kármán constant κ_g may be a more sensitive indicator than those used previously. A consequence of this transition is that we cannot use a single scaling expression for turbulent flow across the entire Reynolds number range. This is important for CFD and other industrial applications.

Fluctuating and mean velocities have been treated separately and combined to calculate the TI. Scaling with Reynolds number and the impact of wall roughness is only seen for the mean flow. We have applied a novel method to derive two-parameter radial expressions using both log- and power-law functions; they capture the main features of the Princeton Superpipe measurements equally well. However, we would tend to recommend using log-law functions since they become universal for high Reynolds numbers.

We have shown that the area-averaged square of the TI is proportional to the friction factor, the proportionality constant being the local von Kármán constant $\kappa_l = 0.39$.

ACKNOWLEDGMENTS

We thank Professor Alexander J. Smits for making the Princeton Superpipe data publicly available.

DATA AVAILABILITY

Data sharing is not applicable to this article as no new data were created or analyzed in this study.

REFERENCES

1. F. Russo and N. T. Basse, “Scaling of turbulence intensity for low-speed flow in smooth pipes,” *Flow Meas. Instrum.* **52**, 101–114 (2016).
2. N. T. Basse, “Turbulence intensity and the friction factor for smooth- and rough-wall pipe flow,” *Fluids* **2**, 30 (2017).
3. N. T. Basse, “Turbulence intensity scaling: A fugue,” *Fluids* **4**, 180 (2019).
4. M. Hultmark, M. Vallikivi, S. C. C. Bailey, and A. J. Smits, “Logarithmic scaling of turbulence in smooth- and rough-wall pipe flow,” *J. Fluid Mech.* **728**, 376–395 (2013).
5. See <https://smits.princeton.edu/superpipe-turbulence-data/> for Princeton Superpipe (accessed 1 June 2021).
6. I. Marusic, J. P. Monty, M. Hultmark, and A. J. Smits, “On the logarithmic region in wall turbulence,” *J. Fluid Mech.* **716**, R3 (2013).
7. H. K. Versteeg and W. Malalasekera, *An Introduction to Computational Fluid Dynamics: The Finite Volume Method*, 2nd ed. (Pearson, 2007).
8. A. Corbetta, V. Menkovski, R. Benzi, and F. Toschi, “Deep learning velocity signals allow quantifying turbulence intensity,” *Sci. Adv.* **7**, eaba7281 (2021).
9. B. E. Launder and D. B. Spalding, “The numerical computation of turbulent flows,” *Comput. Methods Appl. Mech. Eng.* **3**, 269–289 (1974).
10. ANSYS Fluent User’s Guide. Release 2021 R1, Section 7.4.2.1.3, p. 1190.
11. Siemens Simcenter STAR-CCM+ User Guide. Release 2021.1, Design Exploration, Adjoint Shape Optimization: Surface Sensitivity for S-Bend, p. 11068.
12. A. A. Townsend, *The Structure of Turbulent Shear Flow*, 2nd ed. (Cambridge University Press, 1976).
13. F. Durst, J. Jovanović, and J. Sender, “LDA measurements in the near-wall region of a turbulent pipe flow,” *J. Fluid Mech.* **295**, 305–335 (1995).
14. D. I. Pullin, M. Inoue, and N. Saito, “On the asymptotic state of high Reynolds number, smooth-wall turbulent flows,” *Phys. Fluids* **25**, 015116 (2013).
15. N. T. Basse, “A correction term for the asymptotic scaling of drag in flat-plate turbulent boundary layers,” [arXiv:2007.11383](https://arxiv.org/abs/2007.11383) (2021).
16. M. V. Zagarola, A. E. Perry, and A. J. Smits, “Log laws or power laws: The scaling in the overlap region,” *Phys. Fluids* **9**, 2094–2100 (1997).
17. M. V. Zagarola and A. J. Smits, “Mean-flow scaling of turbulent pipe flow,” *J. Fluid Mech.* **373**, 33–79 (1998).
18. H. R. Anbarlooei, D. O. A. Cruz, and F. Ramos, “New power-law scaling for friction factor of extreme Reynolds number pipe flows,” *Phys. Fluids* **32**, 095121 (2020).
19. *A Voyage through Turbulence*, edited by P. A. Davidson, Y. Kaneda, K. Moffatt, and K. R. Sreenivasan (Cambridge University Press, 2011).
20. I. Marusic, R. Mathis, and N. Hutchins, “High Reynolds number effects in wall turbulence,” *Int. J. Heat Fluid Flow* **31**, 418 (2010).
21. V. Yakhot, S. C. C. Bailey, and A. J. Smits, “Scaling of global properties of turbulence and skin friction in pipe and channel flows,” *J. Fluid Mech.* **652**, 65–73 (2010).
22. S. A. Dixit, A. Gupta, H. Choudhary, A. K. Singh, and T. Prabhakaran, “A new universal model for friction factor in smooth pipes,” *Phys. Fluids* **33**, 035134 (2021).
23. *Aerodynamic Theory*, edited by W. F. Durand (California Institute of Technology, 1943), Vol. III.

- ²⁴N. Skouloudis and Y. Hwang, “Scaling of turbulence intensities up to $Re_\tau = 10^6$ with a resolvent-based quasilinear approximation,” *Phys. Rev. Fluids* **6**, 034602 (2021).
- ²⁵M. Wosnik, L. Castillo, and W. K. George, “A theory for turbulent pipe and channel flows,” *J. Fluid Mech.* **421**, 115–145 (2000).
- ²⁶H. M. Nagib and K. A. Chauhan, “Variations of von Kármán coefficient in canonical flows,” *Phys. Fluids* **20**, 101518 (2008).
- ²⁷I. Marusic, B. J. McKeon, P. A. Monkewitz, H. M. Nagib, and A. J. Smits, “Wall-bounded turbulent flows at high Reynolds numbers: Recent advances and key issues,” *Phys. Fluids* **22**, 065103 (2010).
- ²⁸R. Deshpande, J. P. Monty, and I. Marusic, “Active and inactive components of the streamwise velocity in wall-bounded turbulence,” *J. Fluid Mech.* **914**, A5 (2021).
- ²⁹P. A. Davidson, *Turbulence—An Introduction for Scientists and Engineers* (Oxford University Press, 2004).
- ³⁰H. Schlichting and K. Gersten, *Boundary-Layer Theory*, 8th ed. (Springer, 2000).
- ³¹N. Tillmark and P. H. Alfredsson, “Experiments on transition in plane Couette flow,” *J. Fluid Mech.* **235**, 89–102 (1992).
- ³²X. Chen and K. R. Sreenivasan, “Reynolds number scaling of the peak turbulence intensity in wall flows,” *J. Fluid Mech.* **908**, R3 (2021).
- ³³P. A. Monkewitz, “Asymptotics of stream-wise Reynolds stress in wall turbulence,” [arXiv:2104.07322](https://arxiv.org/abs/2104.07322) (2021).
- ³⁴I. Marusic, W. J. Baars, and N. Hutchins, “Scaling of the streamwise turbulence intensity in the context of inner–outer interactions in wall turbulence,” *Phys. Rev. Fluids* **2**, 100502 (2017).
- ³⁵S. B. Pope, *Turbulent Flows* (Cambridge University Press, 2000).
- ³⁶G. I. Barenblatt, “Scaling laws for fully developed turbulent shear flows. Part 1. Basic hypotheses and analysis,” *J. Fluid Mech.* **248**, 513–520 (1993).
- ³⁷G. I. Barenblatt and V. M. Prostokishin, “Scaling laws for fully developed turbulent shear flows. Part 2. Processing of experimental data,” *J. Fluid Mech.* **248**, 521–529 (1993).